

Realization of super-bunching laser with giant high-order correlations and extreme photon-number fluctuations

Chengbing Qin^{1,2,3,*},†, Yuanyuan Li^{1,2},†, Yu Yan³,†, Jiamin Li^{3,*}, Xiangdong Li^{1,2}, Yunrui Song^{1,2}, Xuedong Zhang^{1,2}, Shuangping Han³, Zihua Liu³, Yanqiang Guo^{3,4}, Guofeng Zhang^{1,2}, Ruiyun Chen^{1,2}, Jianyong Hu^{1,2}, Zhichun Yang^{1,2}, Xinhui Liu^{1,2}, Liantuan Xiao^{1,2,3,4,*}, and Suotang Jia^{1,2}

1. State Key Laboratory of Quantum Optics and Quantum Optics Devices, Institute of Laser Spectroscopy, Shanxi University, Taiyuan, Shanxi 030006, China
2. Collaborative Innovation Center of Extreme Optics, Shanxi University, Taiyuan, Shanxi 030006, China
3. Department of Physics and Optoelectronics, Taiyuan University of Technology, Taiyuan, 030024, China
4. Key Laboratory of Advanced Transducers and Intelligent Control System of Ministry of Education, Taiyuan University of Technology, Taiyuan, 030024, Shanxi, China

* Corresponding authors. Email:

Chengbing Qin, chbqin@sxu.edu.cn;

Jiamin Li, lijiamin@tyut.edu.cn;

Liantuan Xiao, xlt@sxu.edu.cn

† These authors contributed equally to this work.

Abstract

Non-classical light sources emitting bundles of N -photons have essential applications ranging from fundamental tests to quantum information processing. However, high-order correlations, $g^{(N)}(0)$ ($N \geq 2$), are still limited to hundreds. Herein, we report the realization of a super-bunching laser in a photonic crystal fiber with $g^{(2)}(0)$ reaching 5.86×10^4 and $g^{(5)}(0)$ reaching 2.72×10^8 . This laser presented extreme photon-number fluctuations and ubiquitous multi-photon events, with the occurrence of 31 photons from a single light pulse at a mean of 1.99×10^{-4} photons per pulse. The probability of this extreme event has been enhanced 10^{139} times compared to a coherent laser with a Poissonian distribution. By varying the power of the pumping laser, both the photon number distributions and the corresponding high-order correlations could be substantially tailored from Poissonian to super-bunching distributions. Our study showcases the ability to achieve non-classical laser with giant high-order correlations and extreme photon-number fluctuations, paving the way for high-order correlation imaging, extreme nonlinear optical effects, hyperspectral image and multi-photon physics.

Keywords: super-bunching laser, second order correlation, photon number probability distribution, multi-photon events, N-photon bundle emission, photonic crystal fiber

1. Introduction

Quantum optics was born from the study of photon statistics. The statistical properties of a light beam can be characterized using the second-order correlation function, $g^{(2)}(\tau)$, first proposed by Hanbury Brown and Twiss (1, 2). Shortly after, Glauber (3) introduced a quantum mechanical description of the second-order correlation function. The normalized $g^{(2)}(0)$, an essential tool for quantum state classification, aiming at recognizing what kind of photon number distributions the investigated light source emits, can be distinguished into sub-Poissonian [$g^{(2)}(0) < 1$], Poissonian [$g^{(2)}(0) = 1$], and super-Poissonian [$1 < g^{(2)}(0)$] distributions (4-6), which are also known as anti-bunching, coherent, and bunching emissions, respectively. Super-bunching light sources with $g^{(2)}(0) > 2$ indicate the existence of correlated photons or a multi-photon bundle emission and also suggest extreme photon-number fluctuations stronger than those of thermal light. Such highly non-classical states of light are of fundamental interest to quantum optics and constitute a starting point for engineering more complex quantum states. They are also essential for newly emerging, more resource-efficient photonic architectures for universal quantum computation and quantum error correction using individual, higher-dimensional systems, as well as for the optimal capacity of a quantum communication channel and Heisenberg limited quantum metrology (interferometry) (7-13). Furthermore, the efficiency of multi-photon nonlinear light-matter interactions, such as two-photon absorption, is proportional to the bunching peak $g^{(N)}(0)$ of the light field, which has been experimentally verified with both thermal light and entangled photon pairs (14-16). Therefore, the super-bunching effect of light fields is of essential importance not only from the viewpoint of fundamental physics but also for applications such as quantum communications, computation, and nonlinear optics. Although the super-bunching effect has been observed in various systems, such as parametric down-conversion (17, 18), quantum dots (19, 20), atomic ensembles (21), superconducting circuits (22), and generic tunnel junctions (23), the existing super-bunched photon sources generally suffer from either low quantum yields, small N-photon bundle emission, weak photon number fluctuations, or low super-bunching index values ($g^{(2)}(0)$ limited to hundreds) (24).

In this study, we realized a giant super-bunching effect from a supercontinuum laser, with $g^{(2)}(0)$ reaching 5.86×10^4 in the visible region, through the nonlinear interactions between a low-power pump laser and a photonic crystal fiber (PCF). High-order correlation functions of the laser were obtained, with $g^{(5)}(0)$ reaching 2.72×10^8 , at least six orders of magnitude higher than that of the thermal light (25, 26). The measurement of the photon number probability distribution, uncovered by a home-made photon-number-resolving single-photon counting module (SPCM) array, demonstrated that the photon statistics of the light with a giant $g^{(2)}(0)$ were far beyond the coherent (Poissonian) and thermal (Bose-Einstein) distributions and presented extreme photon-number fluctuations. The N -photon production probability, scaling as the N th-order normalized correlation functions, was dramatically enhanced. Compared with coherent light, the 31-photon production probability could be

improved 10^{139} times with a mean number of photons per pulse ($\langle n \rangle$) of 1.99×10^{-4} . Counterintuitively, with the decrease in $\langle n \rangle$, the likelihood of bundled photon emission with an enormous N value will increase rather than decline. The extreme photon-number fluctuations and giant high-order correlation were attributed to the parallel nonlinear interaction pumping by a bright squeezed vacuum light, and the simulation results were highly consistent with the experimental results. This super-bunching laser offers unique applications for high-order correlated optical imaging under extreme conditions and new paradigms for optical communications and metrology.

2. Result and discussion

Experimental setup

The experimental layout for the realization and measurement of the super-bunching laser is simplistically depicted in Fig. 1A (see supplementary text S1.1 for details). The super-bunching light was achieved through a PCF with passive and all-fiber configurations. A semiconductor saturable absorber mirror (SESAM) mode-locked fiber laser acted as the seed pulse, successively amplified by a pre-amplifier and a main amplifier. The super-bunching laser was generated by injecting a low-power pump laser into a PCF, which was composed of five layers of periodically arranged air holes, forming a ring-shaped configuration within the fiber (see Fig. S1 for the morphology and dispersion curves). The high-order correlation functions and photon number probability distribution were measured by an array of silicon-based SPCMs and a multi-channel event timer with a time-correlated single-photon counting unit.

Measurement of $g^{(N)}(0)$

The spectral region and emission thresholds of the super-bunching laser could be varied by changing the pump power of the main amplifier. For example, Fig. 1B presents the input–output power curve for this laser with a center wavelength of 605 nm, a bandwidth of 70 nm, and a repetition of 80 MHz. The threshold (P_{th}) for the 605 nm emission was determined to be 1.65 W. As expected and reported previously (27), the value of $g^{(2)}(0)$ for the emission beyond the threshold (*e.g.*, the pump power was three folds of the threshold, $P_{\text{pump}}=3P_{\text{th}}$) was close to 1, the characteristic feature of coherent lights. As the pump power approached the threshold, $g^{(2)}(0)$ tended to 2, the characteristic feature of chaotic light. Surprisingly, the value of $g^{(2)}(0)$ surpassed 2 and favored thousands with the decrease in the pump power (Fig. 1C), and the observed maximum $g^{(2)}(0)$ reached up to 5.86×10^4 (Fig. S5). Fig. 1D presents a typical second-order correlation function with $g^{(2)}(0)=16747$, which is two orders larger than the reported values (28-30), indicating the remarkable non-classical effects of this light source. This result indicates that this light field can be substantially tailored from a coherent to a super-bunching light field. Furthermore, higher-order correlations may provide a detailed understanding of the nature of quantum many-particle states. For example, $g^{(3)}$ and $g^{(4)}$ can provide information about the skewness and kurtosis of the

fluctuation statistics, respectively (31). As shown in Fig. 1E, $g^{(3)}(0)$, $g^{(4)}(0)$, and $g^{(5)}(0)$ reached 9.54×10^4 , 1.29×10^6 , and 2.72×10^8 , respectively, under an intermediate condition with $g^{(2)}(0)=75$ and $\langle n \rangle$ at the 10^{-2} level. The rising tendency for the super-bunching laser followed e^{5N} , indicating that $g^{(31)}(0)$ could reach 10^{67} . Note that the measurement of $g^{(N)}(0)$ with $N > 5$ was restricted by the exponential growth of the photon numbers and the limited computer power, rather than the experimental scheme itself. We also obtained the high-order correlation functions on the coherent and thermal light. As expected, the value of $g^{(N)}(0)$ remained at unity for the coherent light source, and that for the thermal light was close to $N!$, agreeing well with the result of the Bose–Einstein distribution (S1.2 and Fig. S7). The value of $g^{(5)}(0)$ for the super-bunching light source was enhanced by at least six orders of magnitude compared with that of the thermal light, which further manifested the pronounced non-classical effects of our super-bunching laser. Another characteristic feature of the super-bunching laser was that the value of $g^{(N)}(0)$ increased with the decrease in $\langle n \rangle$ (at the same pumping power while using an attenuator, *i.e.*, neutral density filters, to vary $\langle n \rangle$). Note that the value of $g^{(2)}(0)$ improved from 49 to 2284 when $\langle n \rangle$ decreased from 9.44×10^{-3} to 8.68×10^{-5} , and that of $g^{(3)}(0)$ improved from 4354 to 4.99×10^5 when $\langle n \rangle$ decreased from 9.44×10^{-3} to 5.31×10^{-4} (Fig. 1F). These results were completely different from those of the coherent and thermal light with the same $g^{(N)}(0)$ value under different $\langle n \rangle$ values (see S1.3 for the calculations of $g^{(N)}(0)$ and Figs. S4–S11 for the supplementary data).

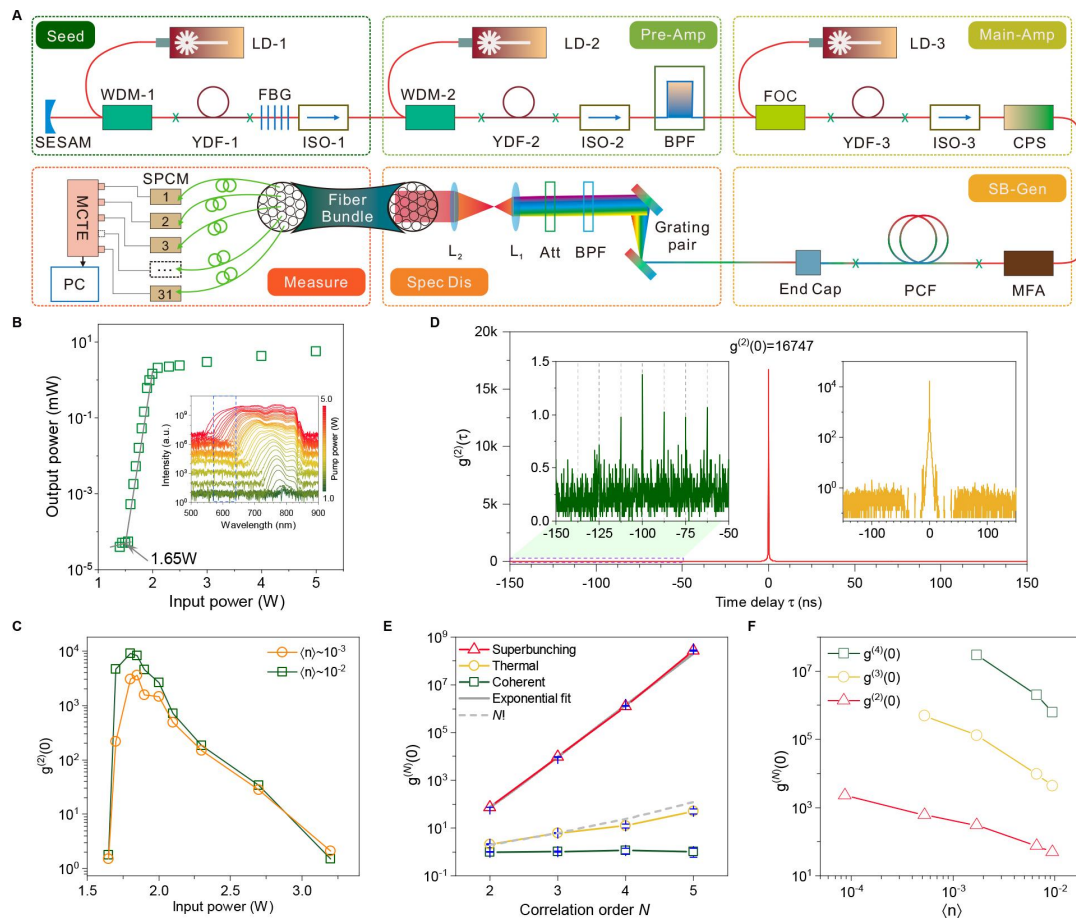


Fig. 1. High-order correlation measurements of the super-bunching laser. (A) Schematic of the realization and measurement of the super-bunching laser. The features of the super-bunching laser could be varied by tuning the pump power of the main amplifier. See S1.1 for details. (B) Output power of the super-bunching laser versus the input pump power of the main amplifier. The inset shows the spectrum evolution in the visible region as a function of the pump power. (C) Measured $g^{(2)}(0)$ as a function of the pump power for two different $\langle n \rangle$ values. (D) Second-order correlation function as a function of the time delay (τ), $g^{(2)}(\tau)$, with $g^{(2)}(0)=16747$. The insets show $g^{(2)}(\tau)$ with a logarithmic scale and an enlargement of $g^{(2)}(\tau)$, with τ between -150 and -50 ns. From the enlargement, bunched and normalized peaks at $\tau=NT$ can be observed with $T=1/f = 12.5$ ns and N as integer values. (E) Measured high-order correlation function $g^{(N)}(0)$ of the super-bunching laser compared with the coherent laser and thermal light. The solid line is an exponential fit of $g^{(N)}(0)$ of the form $11.48 \times e^{5N}$. The short-dashed line is the result of $N!$. (F) $g^{(N)}(0)$ as a function of the mean number of photons per pulse, $\langle n \rangle$. The pumping powers for E and F were 1.85 W. The center wavelength and bandwidth of the super-bunching laser for these measurements were 635 and 70 nm with a repetition frequency of 80 MHz, respectively.

Photon statistics

To uncover the underlying mechanism of the giant $g^{(N)}(0)$, we obtained the photon number probability distribution of the super-bunching laser with 31 SPCMs under different conditions. To check the experimental system, we first performed photon statistics on the conventional pulsed laser. The experimental results were consistent with the theoretical predictions (Fig. S5). For the super-bunching laser, when the pump power was far above the threshold (for instance, $P_{\text{pump}}=3P_{\text{th}}$), the value of $g^{(2)}(0)$ exactly equaled 1, and their photon statistics with $\langle n \rangle$ ranging from 1.37×10^{-1} to 1.97×10^{-4} agreed well with the Poissonian distribution ($P_C(N) = \langle n \rangle^N \cdot e^{-\langle n \rangle} \cdot (N!)^{-1}$, where N and $\langle n \rangle$ are the number of bundled photons and the mean number of photons per pulse), as shown in Fig. 2G. However, when the pump power was close to and especially below the threshold, $g^{(2)}(0)$ had a giant value, and the photon number probability distributions dramatically deviated from the Poissonian distribution. Even with an $\langle n \rangle$ of 4.70×10^{-4} , the probability of a 31-photon bundled emission was still up to 10^{-11} (Fig. 2A). To quantify this deviation, we define the ratio $\zeta_{ij}(N)$ as

$$\zeta_{ij}(N) = \frac{P_i(N)}{P_j(N)} \quad (1)$$

where $P_i(N)$ is the probability of an N -photon bundled emission from the i -type light source within a single pulse. For example, $P_C(31)$ can be understood as the probability of a 31-photon bundled emission within a single pulse from a coherent laser. $\zeta_{SC}(N)$ is

the ratio of $P(N)$ between a super-bunching and coherent laser. It can be demonstrated that, with $g^{(2)}(0)=1$, the values of $\zeta_{sc}(N)$ were limited to values in the range of 1–10 (Fig. 2H), which was mainly due to the limited acquisition time and thus the measurement errors. While with $g^{(2)}(0)$ improving to 347 ($\langle n \rangle=1.89 \times 10^{-1}$), the value of $\zeta_{sc}(31)$ reached up to 10^{53} and presented extremely strong photon-number fluctuations, as shown in Fig. 2D. The maximum $\zeta_{sc}(N)$ value in the experiment reached up to 10^{139} with an $\langle n \rangle$ of 1.99×10^{-4} and $g^{(2)}(0)$ of 3859, as shown in Fig. S5.

With the decrease in $\langle n \rangle$, $g^{(2)}(0)$ dramatically increased at the same pump power. In addition, $\zeta_{sc}(N)$ also presented a significant enhancement. For example, $\zeta_{sc}(31)$ was improved from 2.13×10^{73} to 1.50×10^{126} as $\langle n \rangle$ decreased from 4.01×10^{-2} to 4.70×10^{-4} (Fig. 2D). These results indicated that the probability of an N -photon bundled emission for extremely small $\langle n \rangle$ values could be dramatically enhanced, meaning that small-probability events might always occur in this case and thus manifests extremely strong photon-number fluctuations. To illustrate this conclusion, we plotted the measured sequences of the multi-photon events of the super-bunching laser with $g^{(2)}(0)=4538$ and $\langle n \rangle=1.11 \times 10^{-3}$ in 1 s, as depicted in Figs. S12–S15. We found that the multi-photon events could be easily distinguished, and the extreme events continued to occur, even with the photons exceeding their mean values ($N/\langle n \rangle$) of more than 2.8×10^4 . For comparison, we also plotted the photon sequences of the coherent laser with $\langle n \rangle=4.94 \times 10^{-3}$, where only three 3-photon bundled emissions occurred in 1 s. Fig. 2B presents the variations of $\langle n \rangle$ and $P(N)$ with the pump power. As expected, these two values intuitively increased with the rise of the pump power (the maximum pump powers were slightly larger than P_{th}). In contrast, the values of $\zeta_{sc}(N)$ presented the reverse variation trend, *i.e.*, $\zeta_{sc}(N)$ decreased with the rise of the pump power. This phenomenon indicated that the weaker the pump power was, the higher the N -photon bundle emission generation probability became. Note that when the pump power was much lower than P_{th} , both $P(N)$ and $g^{(2)}(0)$ were close to coherent light due to the extremely weak photon emissions, which were close to Gaussian noise. Another feature of the super-bunching light source was that $P(N)$ and $\zeta_{sc}(N)$ presented the same tendency for similar $\langle n \rangle$ values but rather different pump powers. With $\langle n \rangle$ close to 1.00×10^{-2} as an example (Figs. 2C and 2F), the $\zeta_{sc}(N)$ curves at four pump powers overlapped. Furthermore, we found that the probability of a multi-photon bundled emission (mainly with N between 10 to 25 presented in Figs. 2B and 2C) showed a plateau rather than the “heavy-tail” probability distributions reported previously (30, 32). Counterintuitively, $P(N>25)$ was more extensive than $P(N=25)$ in most cases, suggesting the divergent feature of the probability distributions. To explore this phenomenon, we selected a convergent probability distribution and performed photon statistics with arbitrary M channels ($M \leq 31$). The results are shown in Fig. S17. “Upturned-tail” distributions were observed when the number of SPCM channels decreased. Hence, the “upturned-tail” distributions principally originated from N -photon bundle emissions with $N>M$. This result hinted that the multi-photon bundle emission exceeded 31 in our experiment.

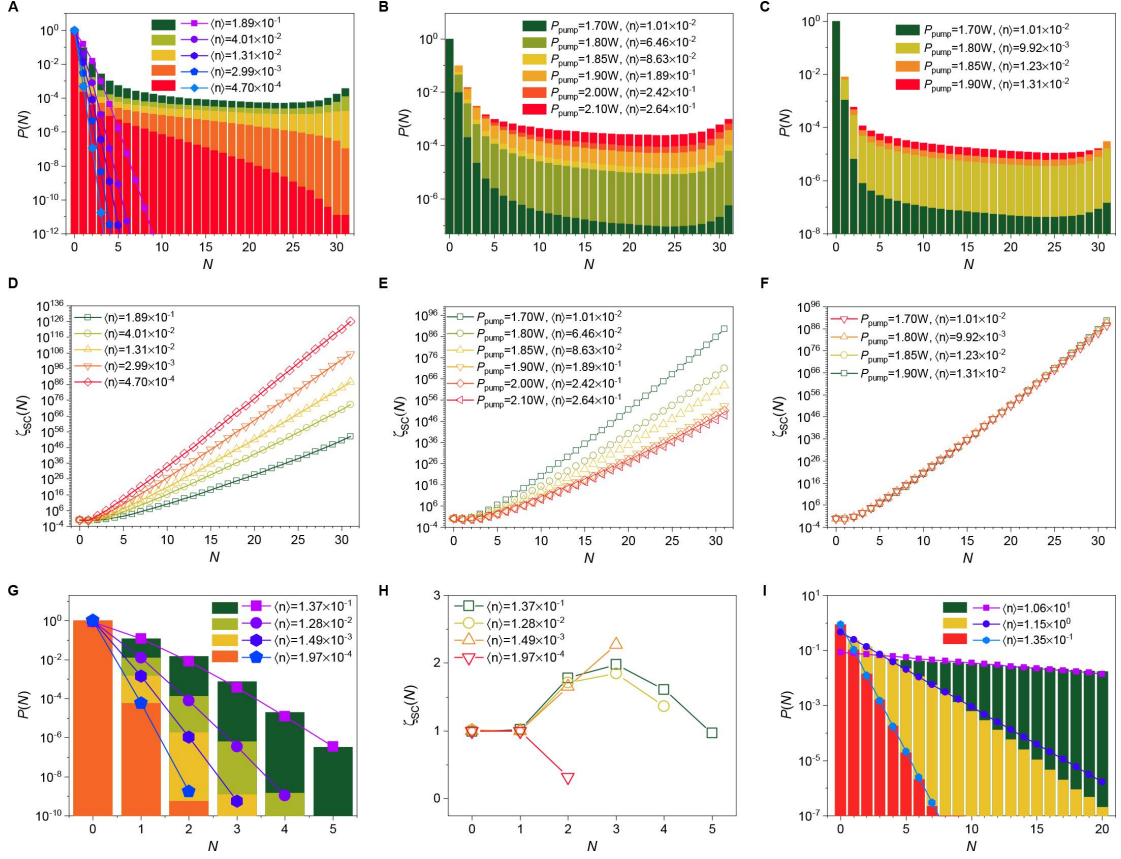


Fig. 2. Photon number probability distribution measurement, $P(N)$. (A) $P(N)$ of the super-bunching laser with different mean numbers of photons per pulse, $\langle n \rangle$, at a pump power of 1.85 W. The mean number was varied using neutral density filters. The solid symbols represent the Poissonian distributions with the same $\langle n \rangle$ value. With the decrease in $\langle n \rangle$, the $g^{(2)}(0)$ values are 347, 1562, 2811, 4573, and 11637. (B) $P(N)$ at different pump powers without decay. The $\langle n \rangle$ value under each pump power has been denoted. With the increase of pump power, the $g^{(2)}(0)$ values are 215, 288, 595, 347, 191, and 145. (C) $P(N)$ with similar $\langle n \rangle$ values and different pump powers. With the increase of pump power, the $g^{(2)}(0)$ values are 215, 3024, 3609, and 2811. The corresponding ratios of $P(N)$ between the super-bunching and coherent lasers ($\zeta_{sc}(N)$) in (A), (B), and (C) are shown in (D), (E), and (F), respectively. (G) $P(N)$ of the super-bunching laser with various $\langle n \rangle$ values at $P_{\text{pump}} = 4.5$ W and $g^{(2)}(0) = 1.05$. The solid symbols represent the Poissonian distributions. (H) $\zeta_{sc}(N)$ for the super-bunching laser in (G). (I) $P(N)$ of the thermal light with various $\langle n \rangle$ values and $g^{(2)}(0) \sim 2.0$. The solid symbols are the simulated Bose–Einstein distributions. See Figs. S8–S10 for further information.

To further illustrate the extremely fluctuating feature of the super-bunching laser, we also obtained the photon number distribution of a thermal light, as shown in Fig. 2I, which agreed closely with Bose–Einstein statistics ($P_T(N) = \langle n \rangle^N / (1 + \langle n \rangle)^{N+1}$, see S1.2 and Fig. S7 for details). Moreover, the $g^{(2)}(0)$ value for the thermal light was close to 2. These two features agreed well with the theoretical predictions. The ratios

of the $P(N)$ values between the thermal and coherent light, $\zeta_{TC}(N)$, increased exponentially with the increase in the photon number for small $\langle n \rangle$ values, due to the “heavy-tailed” distributions in thermal light sources. Although $\zeta_{TC}(N)$ exhibited a similar tendency, the maximum value was limited to 10^{12} , at least 30 orders of magnitude smaller than that of the super-bunching laser with a similar $\langle n \rangle$ value.

Proposed mechanism and simulation

The extreme multi-photon events and giant high-order correlations can be attributed to the synchronized and complicated nonlinear interactions between the PCF and the pump laser. Typically, the nonlinear effects in the PCF can be subdivided into two main categories: phenomena induced by the nonlinearities that arise from scattering (stimulated Brillouin scattering and stimulated Raman scattering) and those induced by the nonlinear effects due to the Kerr effect (self-phase modulation, cross-phase modulation, four-wave mixing, and modulation instability, as shown in Figs. 3A–3C.) (33, 34). These nonlinear effects resulted in spectral broadening and the realization of correlated photon pairs with different wavelengths. Under a pumping laser, these correlated photon pairs would overlap, forming a quantum state known as a “bright squeezed vacuum (BSV)” (35, 36). The electric field quadratures of the BSV have different quantum uncertainties, one below the vacuum level (squeezed) and the other anti-squeezed (Fig. 3D). Due to the anti-squeezed feature and the presence of correlated photon pairs, BSV light shows super-bunched photon statistics, whose photon number probability distribution can be expressed as follows (30, 35, 36):

$$P_{BSV}(N) = \frac{1}{\sqrt{2\pi\langle n \rangle N}} \cdot e^{-N/2\langle n \rangle} \quad (2)$$

This formula offers an extensive and heavy-tailed distribution. Under weak pumping, the BSV light exhibited a strong squeezed feature. Also, none of the above-mentioned nonlinear interactions showed a particular advantage in this case. Using the BSV to pump the PCF with these synchronized nonlinear effects resulted in a super-bunching laser, of which the photon distribution was beyond the BSV and is given as follows (30, 36):

$$P_S(N) = \frac{\exp\left(-\frac{\operatorname{arcsinh}\sqrt{N}}{2\kappa\langle n_B \rangle}\right)}{\sqrt{8\pi\kappa\langle n_B \rangle \cdot N(1+N)\operatorname{arcsinh}\sqrt{N}}} \quad (3)$$

where κ the conversion efficiency of nonlinear interactions (such as four-wave mixing process), n_B is the number of BSV photons. Fig. 3F shows the simulation results with different $\langle n \rangle$ values, uncovering a broad photon distribution (see S1.4 and Fig. S18 for details). The simulation results were far beyond Poissonian and Bose–Einstein distributions but consistent with the experiments. To further support this conclusion, we compared the theoretical predictions with the experimental results with the same $\langle n \rangle$ value (Fig. 3G), which showed that the approximations were reasonable. We also

calculated $g^{(2)}(0)$ for the super-bunching laser with and without Gaussian noise, as shown in Fig. 3H. Here, the Gaussian noise can be treated as the coherent emission from the PCF. The super-bunching laser presented giant $g^{(2)}(0)$ values and increased with the decrease in $\langle n \rangle$. With certain Gaussian noise, $g^{(2)}(0)$ presented maximum values. These simulations agreed well with the experiments, further proving the accuracy of the theoretical model. In contrast, under intense pumping ($P_{\text{pump}} > P_{\text{th}}$), the BSV light exhibited a weak squeezed feature and approximated coherent light. Also, some of the nonlinear effects dominated the interaction between the pump laser and the PCF due to their relatively large nonlinear coefficients (Fig. 3E). Therefore, with the increase in the pumping power, both photon distributions and $g^{(2)}(0)$ transferred from the super-bunching laser to a coherent laser.

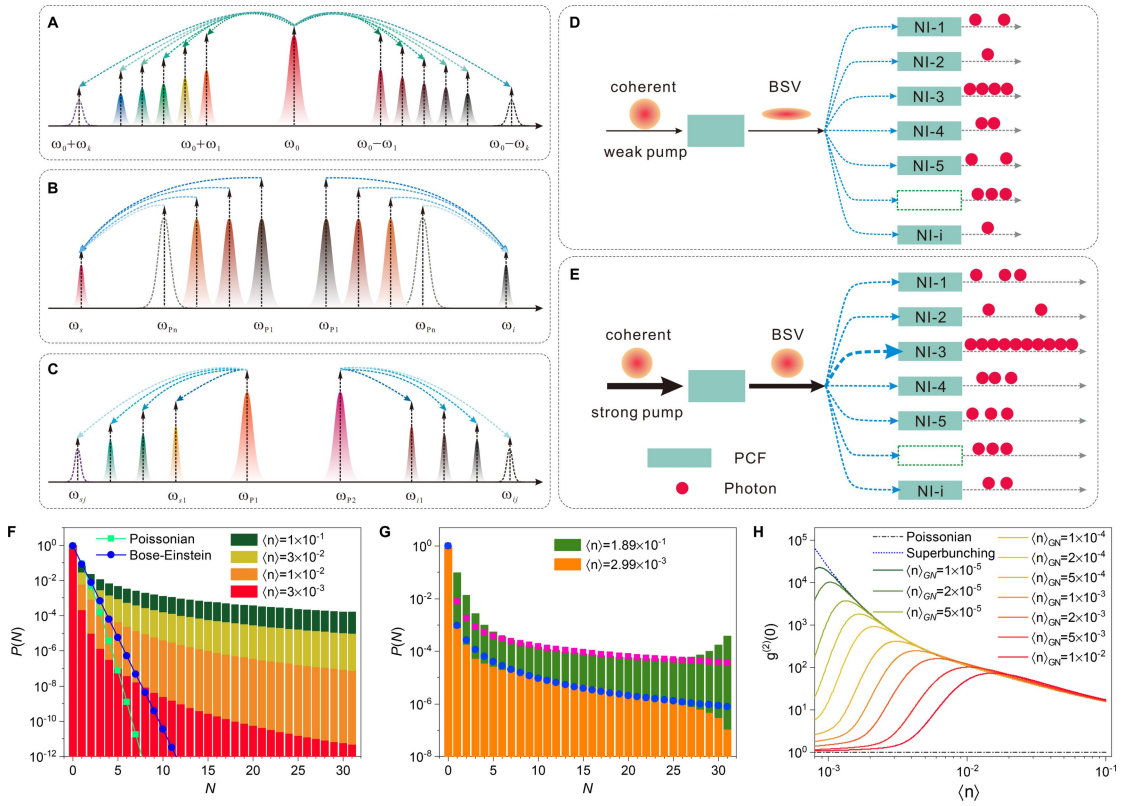


Fig. 3. Proposed mechanism for the realization of the super-bunching laser and theoretical simulations. Schematic representations of the nonlinear interactions (NI) in the PCF (A) self-phase modulation (SPM), (B) cross-phase modulation (XPM), and (C) four-wave mixing (FWM). These nonlinear interactions resulted in the generation of correlated photon pairs. (D) Generation of super-bunching laser by a bright squeezed vacuum (BSV) with robust squeezed features under weak coherent pumping. In this case, various nonlinear interactions might occur synchronously, resulting in extremely strong photon-number fluctuations. (E) Realization of the Poissonian emission through the BSV with weak squeezed features under intense coherent pumpings, where some nonlinear interactions dominated the emission. (F) Theoretical simulations of the photon number probability distributions of the super-bunching laser.

The solid symbols represent the Poissonian and Bose–Einstein distributions with $\langle n \rangle = 1 \times 10^{-1}$. **(G)** Comparisons between the theoretical simulations and experimental results with the same $\langle n \rangle$ value. **(H)** Theoretical predictions of $g^{(2)}(0)$ of the super-bunching laser as a function of $\langle n \rangle$ for different Gaussian noise levels $\langle n \rangle_{GN}$. The dashed and dotted lines represent $g^{(2)}(0)$ for the coherent and super-bunching laser, respectively.

3. Conclusion

In this study, we provided an experimental demonstration of a non-classical laser with giant high-order correlations and an extremely large probability for multi-photon events through the nonlinear interactions between BSV light and a PCF. Both the second-order correlations and photon statistics of this laser can be tailored from Poissonian distributions to super-bunching distributions by varying the power of the pumping laser and/or the mean photons per pulse using neutral density filters. The unparalleled characteristics of the super-bunching laser are especially important for multi-photon correlated imaging, the nonlinear optics of fragile structures, and quantum thermodynamics. For example, the super-bunching laser can be used for extremely weak light detection and ranging as well as communications. Although extremely small $\langle n \rangle$ values will be detected in this case, the accuracy of the information can be determined, and the intense background noise can be eliminated based on multi-photon-correlated calculations or heralding measurements. The extremely high probabilities of multi-photon events are already suitable for practical applications. The occurrence of multi-photon events also results in extremely fluctuating light and offers much more efficiency for multi-photon effects than coherent sources with the same mean number, which has been proven by experiments (15, 32). The super-bunching laser with giant $g^{(N)}(0)$ values may enhance the multi-photon effects by several orders of magnitudes. Furthermore, the super-bunching laser manifests giant high-order correlations for the full broad wavelegths from visible to near-infrared wavelengths (Fig. S6), this feature also beneficial for hyperspectral imaging without any spectrometers(37, 38), only through cross-correlation with different wavelengths.

References and notes

1. R. Hanbury Brown, R. Q. Twiss, A Test of a New Type of Stellar Interferometer on Sirius. *Nature* **178**, 1046-1048 (1956).
2. R. Hanbury Brown, R. Q. Twiss, The Question of Correlation between Photons in Coherent Light Rays. *Nature* **178**, 1447-1448 (1956).
3. R. J. Glauber, Coherent and Incoherent States of the Radiation Field. *Physical Review* **131**, 2766-2788 (1963).
4. Kevin A. Fischer *et al.*, Signatures of two-photon pulses from a quantum two-level system. *Nature Physics* **13**, 649-654 (2017).
5. K. Laiho, T. Dirmeier, M. Schmidt, S. Reitzenstein, C. Marquardt, Measuring higher-order photon correlations of faint quantum light: A short review. *Physics*

- Letters A* **435**, 128059 (2022).
6. E. Zubizarreta Casalengua, J. C. López Carreño, F. P. Laussy, E. d. Valle, Conventional and Unconventional Photon Statistics. *Laser & Photonics Reviews* **14**, 1900279 (2020).
 7. M. J. Holland, K. Burnett, Interferometric detection of optical phase shifts at the Heisenberg limit. *Physical Review Letters* **71**, 1355-1358 (1993).
 8. L. Pezzé, A. Smerzi, Ultrasensitive Two-Mode Interferometry with Single-Mode Number Squeezing. *Physical Review Letters* **110**, 163604 (2013).
 9. J.-W. Pan *et al.*, Multiphoton entanglement and interferometry. *Reviews of Modern Physics* **84**, 777-838 (2012).
 10. T. Nagata, R. Okamoto, J. L. O'Brien, K. Sasaki, S. Takeuchi, Beating the Standard Quantum Limit with Four-Entangled Photons. *Science* **316**, 726-729 (2007).
 11. M. W. Mitchell, J. S. Lundeen, A. M. Steinberg, Super-resolving phase measurements with a multiphoton entangled state. *Nature* **429**, 161-164 (2004).
 12. S. Slussarenko *et al.*, Unconditional violation of the shot-noise limit in photonic quantum metrology. *Nature Photonics* **11**, 700-703 (2017).
 13. C. Groiseau, A. E. J. Elliott, S. J. Masson, S. Parkins, Proposal for a Deterministic Single-Atom Source of Quasisuperradiant N-Photon Pulses. *Physical Review Letters* **127**, 033602 (2021).
 14. A. Nevet, A. Hayat, P. Ginzburg, M. Orenstein, Indistinguishable photon pairs from independent true chaotic sources. *Physical Review Letters* **107**, 253601 (2011).
 15. A. Jechow, M. Seefeldt, H. Kurzke, A. Heuer, R. Menzel, Enhanced two-photon excited fluorescence from imaging agents using true thermal light. *Nature Photonics* **7**, 973-976 (2013).
 16. M. R. Harpham, Ö. Süzer, C.-Q. Ma, P. Bäuerle, T. Goodson, III, Thiophene Dendrimers as Entangled Photon Sensor Materials. *Journal of the American Chemical Society* **131**, 973-979 (2009).
 17. Y. Chang, A. Gonzalez-Tudela, C. Sanchez Munoz, C. Navarrete-Benlloch, T. Shi, Deterministic Down-Converter and Continuous Photon-Pair Source within the Bad-Cavity Limit. *Physical Review Letters* **117**, 203602 (2016).
 18. X. Guo *et al.*, Parametric down-conversion photon-pair source on a nanophotonic chip. *Light Sci Appl* **6**, e16249 (2017).
 19. J. Liu *et al.*, A solid-state source of strongly entangled photon pairs with high brightness and indistinguishability. *Nature Nanotechnology* **14**, 586-593 (2019).
 20. A. Ulhaq *et al.*, Cascaded single-photon emission from the Mollow triplet sidebands of a quantum dot. *Nature Photonics* **6**, 238-242 (2012).
 21. B. Srivathsan *et al.*, Narrow Band Source of Transform-Limited Photon Pairs via Four-Wave Mixing in a Cold Atomic Ensemble. *Physical Review Letters* **111**, 123602 (2013).
 22. S. Gasparinetti *et al.*, Correlations and Entanglement of Microwave Photons Emitted in a Cascade Decay. *Physical Review Letters* **119**, 140504 (2017).

23. C. C. Leon *et al.*, Photon superbunching from a generic tunnel junction. *Science Advances* **5**, eaav4986 (2019).
24. A. M. Berhane *et al.*, Bright Room-Temperature Single-Photon Emission from Defects in Gallium Nitride. *Advanced Materials* **29**, 1605092 (2017).
25. M. Avenhaus, K. Laiho, M. V. Chekhova, C. Silberhorn, Accessing higher order correlations in quantum optical states by time multiplexing. *Physical Review Letters* **104**, 063602 (2010).
26. R. Cheng *et al.*, A 100-pixel photon-number-resolving detector unveiling photon statistics. *Nature Photonics* **17**, 112-119 (2022).
27. J. Wiersig *et al.*, Direct observation of correlations between individual photon emission events of a microcavity laser. *Nature* **460**, 245-249 (2009).
28. Z. Wang *et al.*, Optically Driven Giant Superbunching from a Single Perovskite Quantum Dot. *Advanced Optical Materials* **9**, 2100879 (2021).
29. F. Jahnke *et al.*, Giant photon bunching, superradiant pulse emission and excitation trapping in quantum-dot nanolasers. *Nature Communications* **7**, 11540 (2016).
30. M. Manceau, K. Y. Spasibko, G. Leuchs, R. Filip, M. V. Chekhova, Indefinite-Mean Pareto Photon Distribution from Amplified Quantum Noise. *Physical Review Letters* **123**, 123606 (2019).
31. D. Elvira *et al.*, Higher-order photon correlations in pulsed photonic crystal nanolasers. *Physical Review A* **84**, 061802 (2011).
32. K. Y. Spasibko *et al.*, Multiphoton Effects Enhanced due to Ultrafast Photon-Number Fluctuations. *Physical Review Letters* **119**, 223603 (2017).
33. S. Kumar Orappanpara Soman, A tutorial on fiber Kerr nonlinearity effect and its compensation in optical communication systems. *Journal of Optics* **23**, 123502 (2021).
34. J. M. Dudley, F. Dias, M. Erkintalo, G. Genty, Instabilities, breathers and rogue waves in optics. *Nature Photonics* **8**, 755-764 (2014).
35. A. Gorlach *et al.*, High-harmonic generation driven by quantum light. *Nature Physics* **19**, 1689-1696 (2023).
36. J. Heimerl *et al.*, Multiphoton electron emission with non-classical light. *Nature Physics* **20**, 945-950 (2024).
37. L. Bian *et al.*, A broadband hyperspectral image sensor with high spatio-temporal resolution. *Nature* **635**, 73-81 (2024).
38. F. Yesilkoy *et al.*, Ultrasensitive hyperspectral imaging and biodetection enabled by dielectric metasurfaces. *Nature Photonics* **13**, 390-396 (2019).

ACKNOWLEDGMENTS

Funding: The authors gratefully acknowledge support from the National Key Research and Development Program of China (Grant No. 2022YFA1404201), Natural Science Foundation of China (Nos. U22A2091, 62222509, U23A20380, 62127817, 62075120, 62075122, 62205187, and 62105193), Shanxi Province Science and Technology Innovation Talent Team (No. 202204051001014), the key research and development project of Shanxi Province (202102030201007), and 111 projects (Grant No. D18001).

Author contributions: C. C. Q., J. M. L., and L. T. X. conceived and designed the experiment. C. B. Q., Y. Y. L., Y. Y., and X. D. L. conducted the experiments and analyzed the data. Y. R. S., X. D. Z., S. P. H., G. F. Z., R. Y. C., and J. Y. H. contributed to the optical setup, SPCMs array design, and pseudothermal light preparation. Z. C. Y., X. H. L., and S. T. J. contributed to the electronic measurements and data analysis. J. M. L., Z. H. L., and Y. Q. G. contributed to the theoretical analysis and simulations. C. B. Q., J. M. L., and L. T. X. wrote the manuscript with input from all other authors. C. B. Q. and L. T. X. supervised the project.

Competing interests: The authors declare no competing interests.

Data and materials availability: All data needed to evaluate the conclusions in the paper are present in the paper or the supplementary materials.

License information:

SUPPLEMENTARY MATERIALS

Supplementary Text: S1.1-1.4

Supplementary Figures: Figure S1-S18.